This article has been accepted for publication in a future issue of this journal, but has not been fully edited. Content may change prior to final publication. Citation information: DOI 10.1109/JBHI.2017.2709406, IEEE Journal of Biomedical and Health Informatics

Tooth and Alveolar Bone Segmentation from Dental Computed Tomography Images

Yangzhou Gan, *Member, IEEE,* Zeyang Xia, *Senior Member, IEEE*, Jing Xiong, *Member, IEEE,* Guanglin Li, *Senior Member, IEEE,* and Qunfei Zhao

***Abstract*—Three-dimensional (3D) models of tooth-alveolar bone complex are needed in treatment planning and simulation for computer-aided orthodontics. Tooth and alveolar bone segmentation from computed tomography (CT) images is a fundamental step in reconstructing their models. Due to less application of alveolar bone in conventional orthodontic treatment which may cause undesired side effects, the previous studies mainly focused on tooth segmentation and reconstruction and did not consider the alveolar bone. In this study, we proposed a method to implement both tooth and alveolar bone segmentation from dental CT images for reconstructing their 3D models. Firstly, the proposed method extracted the connected region of tooth and alveolar bone from CT images using a global convex level set model. Then individual tooth and alveolar bone are separated from the connected region based on Radon transform and a local level set model. The experimental results showed that the proposed method could successfully complete both the tooth and alveolar bone segmentation from CT images, and outperformed the state of the art tooth segmentation methods in terms of accuracy. This suggests that the proposed method can be used in reconstructing the 3D models of tooth-alveolar bone complex for precise treatment.**

***Index Terms*—orthodontics, tooth and alveolar bone, image segmentation, level set, computed tomography images**

I. Introduction

IN conventional orthodontic treatment, orthodontists mainly depend on physical cast models to perform diagnosis and treatment planning. With the increasing use of dental computed tomography (CT) images in clinic, it is possible to reconstruct the full three-dimensional (3D) digital models of the tooth and alveolar bone to conduct computer-aided diagnosis and treatment. Tooth and alveolar bone segmentation from CT images is a fundamental step in reconstructing their 3D models.

It is a challenge to segment tooth and alveolar bone from their CT images because of the similar intensities between tooth and alveolar bone, close position of neighboring teeth, and complicated topological structure of both tooth and alveolar bone. Several automatic or semi-automatic methods [1-13] have been developed to segment tooth from dental CT images, and some of them achieved a good segmentation accuracy. These previous methods can be classified into two classes: direct 3D segmentation and two-dimensional (2D) slice-by-slice segmentation. The direct 3D segmentation methods segment tooth volume directly in 3D volumetric space. Akhoondali *et al.* [1] developed an automatic segmentation method based on region growing. Keyhaninejad *et al.* [2] and Hosntalab *et al.* [3] proposed to use 3D region based level set model to extract the tooth volume. Keustermans *et al.* [4] and Hiew *et al.* [5] applied a graph cut algorithm to interactively segment 3D tooth volume. Barone *et al.* [6] developed a novel framework to interactively model the 3D shape of tooth with single-root using 2D contours of target tooth outlined from a set of projected images. Pei *et al.* [7] proposed a 3D exemplar-based random walk method which integrated semi-supervised label propagation and regularization by 3D exemplar registration to segment tooth volume from cone-beam CT (CBCT) images. The 2D slice-by-slice segmentation methods segment tooth contours in each 2D slice of transverse plane. This kind of methods generally uses a tooth contour propagation strategy to automatically initialize the tooth contour of contiguous slices, and users only need to manually initialize the starting slice. Heo and Chae [8] and Wu *et al.* [9] used the B-spline snakes with genetic algorithm to extract tooth contours. The B-spline snakes used in their methods cannot address the topological change of molar contours. The level set method has been broadly used for 2D tooth segmentation due to its advantages in dealing with topological change and contour propagation [10-13]. Gao and Chae [10] proposed a level set model with shape and intensity prior to segment tooth contours and achieved high segmentation accuracy. Yau *et al.* [11] applied the same model to extract root contours. Ji *et al.* [12] modified this model to segment anterior teeth. Gan *et al.* [13]

This work was supported by National Natural Science Foundation of China (No. 61601452), National Key Project of Research and Development Plan of China Inter-governmental Cooperative Science and Technology Project (2016YFE0128000), Guangdong Natural Science Funds for Distinguished Young Scholar (2015A030306020), Major Project of Guangdong Province Science and Technology Department (2014B090919002), Youth Innovation Promotion Association, Chinese Academy of Sciences (2015301), China Postdoctoral Science Foundation (2016M600693), and Shenzhen Research Project (GJHS20160331185913023, GJHS20160331190459402, KQCX2015033117354152).

Y. Gan, Z. Xia, and G. Li are with Shenzhen Institutes of Advanced Technology, Chinese Academy of Sciences, Shenzhen 518055, China, and also with CAS Key Laboratory of Human-Machine Intelligence-Synergy Systems, Shenzhen Institutes of Advanced Technology, Shenzhen 518055, China. (E-mail: yz.gan@siat.ac.cn; zy.xia@siat.ac.cn; gl.li@siat.ac.cn).

J. Xiong is with Shenzhen Institutes of Advanced Technology, Chinese Academy of Sciences, Shenzhen 518055, China. (E-mail jing.xiong@siat.ac.cn)

Q. Zhao is with Department of Automation, Shanghai Jiao Tong University, Shanghai 200240, China. (E-mail: zhaoqf@sjtu.edu.cn).

(Corresponding author: Z. Xia.)

This article has been accepted for publication in a future issue of this journal, but has not been fully edited. Content may change prior to final publication. Citation information: DOI 10.1109/JBHI.2017.2709406, IEEE Journal of Biomedical and Health Informatics

developed a hybrid level set model for accurate root segmentation.

Note that all these previous methods focused on individual tooth segmentation, and did not consider the alveolar bone segmentation due to less application of alveolar bone in conventional orthodontic treatment. Wang *et al.* [14] [15] developed promising methods for tooth and bone tissue segmentation from CT images. However, their methods did not involve the tooth segmentation from alveolar bone, thus cannot be applied for individual 3D model reconstruction of tooth and alveolar bone.

In the treatment planning, the 3D model of alveolar bone is necessary to align tooth roots well since it provides reference for the potential position and direction of root. If only using tooth models to perform a treatment planning, there is a risk that the planned tooth roots may be not surrounded by the alveolar bone and tooth loss will occur after the orthodontic treatment. In addition, tooth movement of orthodontic treatment is implemented through alveolar bone tissue modeling and remodeling under orthodontic force, and the dental biomechanics involves tooth, periodontal ligament, and alveolar bone [16]. Thus, in the dental biomechanics simulation, the 3D model of alveolar bone is also needed.

In this study, we propose a level set based method to segment both tooth and alveolar bone contours slice-by-slice from CT images. The contribution of this study mainly includes the following three points. (1) The proposed method implements both segmentation of individual tooth and alveolar bone. It first segments the bony tissue (including tooth and alveolar bone) from CT images, then individual tooth contours are segmented from the bony tissue to separate tooth and alveolar bone. The bony tissue segmentation not only makes the both segmentation of tooth and alveolar bone being possible but also facilitates the individual tooth segmentation. (2) A local level set model composed of edge detection energy and tooth shape prior is developed to segment tooth contours from bony tissue region. In the edge detection energy, intensity information is integrated into the edge indicator for more accurate tooth contour extraction. (3) An initial tooth contour computation strategy based on tooth contour deformation tendency of adjacent slices is developed to reduce the accumulated error of slice-by-slice segmentation method. Experimental results verified that the proposed method obtained promising performance for both tooth and alveolar bone segmentation, and outperformed state of the art tooth segmentation methods in terms of accuracy.

II. Method

A. Motivation and Overview of the Proposed Method

In recent years, the level set method is increasingly applied to medical image segmentation [17-19]. It is possible to simultaneously segment individual tooth and alveolar bone from CT images using multi-phase level set model [20]. However, due to the complex image condition in root part, each tooth needs to be segmented applying an individual level set [10]. Thus, using the multi-phase level set strategy, there needs at most 17 coupled level sets (16 for teeth and 1 for alveolar bone) which are complicated and low efficiency.

Instead of using multi-phase level sets, this study develops a two-step method to segment both tooth and alveolar bone. The procedure of the two-step method is shown in Fig. 1. In the first step, bony tissue is segmented using a global convex level set model. The region with the largest volume in the segmented bonny tissue is the connected region of tooth and alveolar bone. Then the connected region is segmented into independent tooth and alveolar bone. In this step, tooth region is regarded as foreground and segmented slice-by-slice from alveolar bone by applying the Radon transform and a local level set model. Tooth contour propagation strategy that uses segmented tooth contours of previous three slices as the tooth shape prior of current slice is employed to automatically initialize the level set curve.

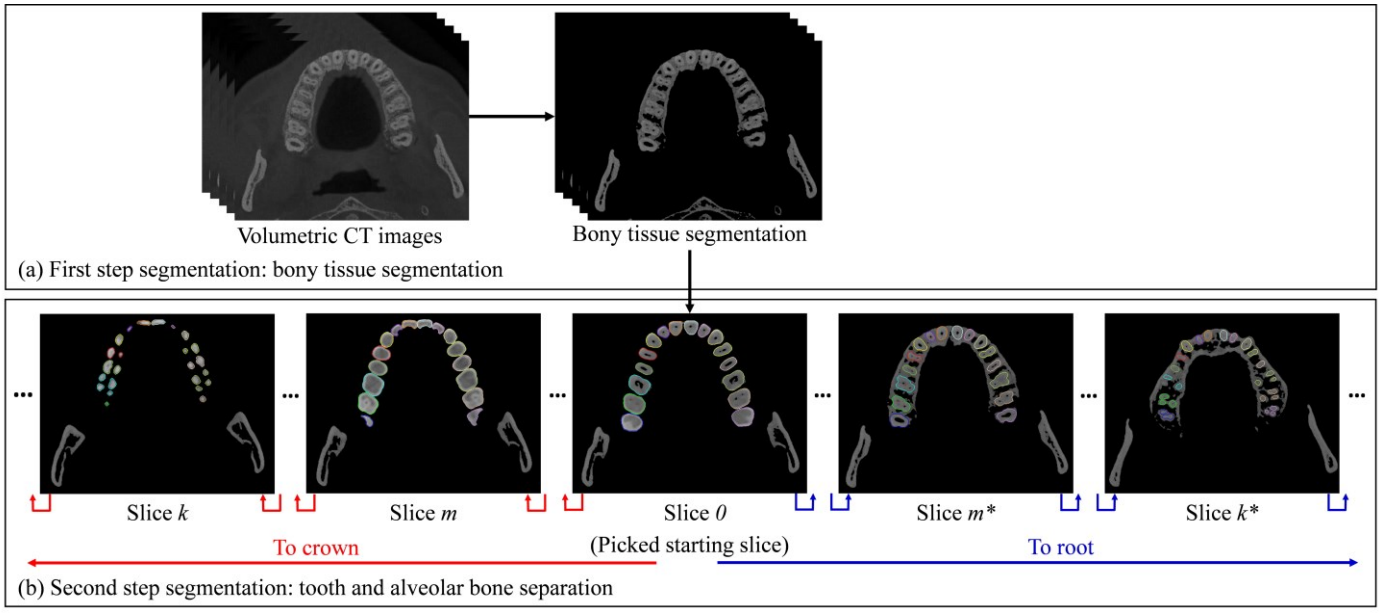

Fig. 1. Procedure of the proposed two-step method for the segmentation of tooth and alveolar bone from CT images.

This article has been accepted for publication in a future issue of this journal, but has not been fully edited. Content may change prior to final publication. Citation information: DOI 10.1109/JBHI.2017.2709406, IEEE Journal of Biomedical and Health Informatics

B. The Global Convex Level Set Model for Bony Tissue Segmentation

In this study, the local binary fitting (LBF) model [21] that has achieved a promising performance for weak edge extraction in the presence of intensity inhomogeneity is adopted to extract the bony tissue. Let $\Omega \in \Re^2$ be the image plane, I: $\Omega \to \Re$ be the given gray image, and ϕ: $\Omega \to \Re$ be a 2D level set function, the energy function of the LBF model is defined as

$$E(\phi) = \sum_{i=1,2} \int\int K_\sigma(x-y)\left|I(y)-f_i(x)\right|^2 M_i(\phi(y))dydx + \mu\int \delta_\varepsilon(\phi)\left|\nabla\phi\right|dx \tag{1}$$

where $x, y \in \Re^2$ denote a point in the image plane, μ is a positive weight, K_σ is a Gaussian Kernel with a scale parameter σ, $f_i(x)$ is the local mean intensities inside and outside the zeros level set, δ_ε is the normalized Dirac delta function [22], and $M_1(\phi)=H_\varepsilon(\phi)$, $M_2(\phi)=1-H_\varepsilon(\phi)$, where H_ε is the normalized Heaviside function [22].

The minimization of energy function (1) with respect to ϕ can be achieved by solving the gradient descent flow equation:

$$\frac{\partial\phi}{\partial t} = -\delta_\varepsilon(\phi)\sum_{i=1,2}(-1)^{i-1}\lambda_i\int K_\sigma(y-x)\left|I(x)-f_i(y)\right|^2 dy + \mu\delta_\varepsilon(\phi)div\left(\frac{\nabla\phi}{|\nabla\phi|}\right) \tag{2}$$

where $t \geqslant 0$ is the artificial iterative time, $div(\cdot)$ denotes the divergence operator, and the local mean intensities f_1 and f_2 are calculated before every iteration using the following equations:

$$f_1(x) = \frac{K_\sigma(x)*\left(H(\phi(x))I(x)\right)}{K_\sigma(x)*\left(H(\phi(x))\right)} \tag{3}$$

$$f_2(x) = \frac{K_\sigma(x)*\left((1-H(\phi(x)))I(x)\right)}{K_\sigma(x)*\left(1-H(\phi(x))\right)} \tag{4}$$

Note that the LBF model would be sensitive to the initial condition due to the fact that the energy function (1) is non-convex which may converge toward local minima. In addition, the minimization procedure of the energy function using the gradient decent scheme would be time consuming. To address the two problems, the global convex segmentation method proposed by Chan *et al.* [23] was adopted and the global convex version of the LBF model was obtained as:

$$\min_{0\le u\le 1}\left\{\int g\left|\nabla u\right|dx + \lambda\int\left(e_1(x)-e_2(x)\right)u(x)dx\right\} \tag{5}$$

where $e_{i=1,2}(x) = \int K_\sigma(x-y)\left|I(y)-f_i(x)\right|^2 dy$, and g is an edge indicator defined as

$$g(x) = \frac{1}{1+|\nabla G_s * I(x)|^2} \tag{6}$$

where $G_s*I(x)$ denotes the smoothed image by convolving I with the Gaussian kernel G_s, and ∇ denotes the differential operator.

Let Ω_C denote the region inside the level set curve, it can be derived that if $u(x)$ is the minimum of (5) for almost every $\alpha \in [0, 1]$, $\Omega_C=\{x: u(x) \geq \alpha\}$ would be the global minimum of (1). To determine the global minimum of (1), one can solve the minimization of (5), and then set $\Omega_C=\{x: u(x) \geq \alpha\}$ for any $\alpha \in [0, 1]$.

The convex constrained minimization problem (5) has unique minimum which can be solved by various minimization technologies. In this study we use the Split Bregman method [24] to solve it. Instead of solving the constrained minimization problem directly, the Split Bregman method introduces an auxiliary vector and a Bregman vector, and then solves a sequence of unconstrained problems. More details on the implementation of the Split Bregman method can be found in Ref. [24].

C. Individual Tooth and Alveolar Bone Segmentation

It is a big challenge to segment individual tooth from alveolar bone due to the several reasons. (1) Tooth has a flexible topological structure and may split into different branches in both root and crown part. (2) Neighboring teeth may touch each other in crown part. (3) Tooth root and alveolar bone connect each other and have similar CT image intensity. In the proposed method, different branches of tooth split naturally after the first step segmentation. The other two difficulties are addressed as follows. (1) Considering that the tooth structure in the mesial-distal side of the crown part is convex and neighboring crowns can be separated using a plane, the Radon transform is applied to calculate a line to separate neighboring teeth in each slice. (2) A local level set model integrated edge detection energy and tooth shape prior is developed to segment tooth contours from alveolar bone.

In the implementation, individual tooth is segmented from alveolar bone slice-by-slice semi-automatically. Firstly, a starting slice is selected manually from crown part, and a seed point of each tooth is drawn in the starting slice for the detection of valid tooth region [13]. Then, all the images are segmented slice-by-slice automatically along the crown or root direction based on tooth contour propagation strategy. The propagation strategy uses the segmented tooth contours of the previous three slices as the tooth shape prior to automatically initialize the tooth contour. For each slice segmentation, a line is first extracted to separate neighboring teeth into independent ones using the Radon transform. Then, each tooth is segmented from the region of the corresponding side of the line using a local level set model.

1) Tooth Contour Propagation Strategy

A natural propagation strategy has been used which applied the segmented contour of previous slice as the tooth shape prior of current slice to be segmented [10], but suffers from serious accumulated error. To reduce the accumulated error, Wu *et al.* [25] used the average shape of the previous three segmented slices as the shape prior. Their results showed that the average strategy is effective to reduce the accumulated error, but the

This article has been accepted for publication in a future issue of this journal, but has not been fully edited. Content may change prior to final publication. Citation information: DOI 10.1109/JBHI.2017.2709406, IEEE Journal of Biomedical and Health Informatics

computed tooth shape prior may be inaccurate. This study applied the shrinking or expansion deformation tendency of tooth contours to compute the tooth shape prior.

Tooth anatomical structure (shown in Fig. 2) indicates that in a certain direction especially in lingual and buccal direction, when the tooth contour moves from tooth neck part to root or crown part, it has a shrinking or expansion deformation tendency. This study applied the deformation tendency to pixel-wisely detect whether the segmentation of the previous slice occur error. If there was no segmentation error, the segmented contour of the previous slice would be directly used as the tooth shape prior. Otherwise, the tooth shape prior would be computed by averaging the segmented contours of previous three slices.

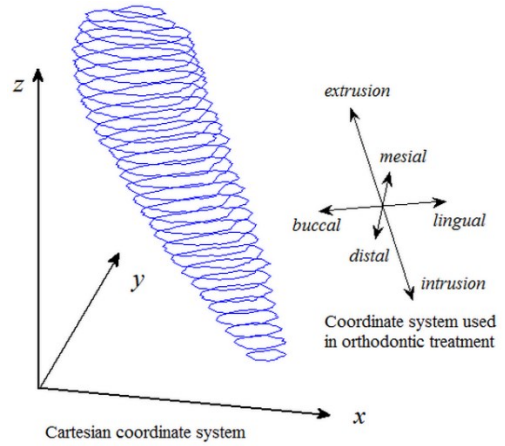

Fig. 2. Structure of the tooth contours in 3D space.

Let ϕ_{i-1}, ϕ_{i-2}, and ϕ_{i-3} be the level set functions of segmented tooth contours of the previous three slices, respectively. For a given point x, if $(\phi_{i-2}(x)-\phi_{i-1}(x))(\phi_{i-3}(x)-\phi_{i-2}(x))\geq 0$, the tooth contours near the point have a shrinking or expansion deformation tendency; otherwise, there is no shrinking or expansion deformation tendency, and segmentation error might occur. This study applies the following expression to compute the tooth shape prior (embedded in a binary mask)

$$S_0(x)=\begin{cases} B\left(\phi_{i-1}(x)\right) & \text{if } \phi_{12}(x)\phi_{23}(x)\geq 0; \\ B\left(\phi_{i-1}(x)+\phi_{i-2}(x)+\phi_{i-3}(x)\right) & \text{else.} \end{cases} \tag{7}$$

where $\phi_{12}=\phi_{i-2}-\phi_{i-1}$, $\phi_{23}=\phi_{i-3}-\phi_{i-2}$, and $B(x)$ is a threshold operator with threshold value 0.

Fig. 3 shows the comparison of obtained shape priors using different strategies. Fig. 3 (a) presents the segmented tooth contours of the previous three slices that are designated as red, green, and blue curves, respectively. It can be seen that the red curve occurs a boundary leakage error. Fig. 3 (b) presents the computed shape priors using different strategies, in which the red, white, and yellow curves represent the results obtained by using Gao *et al.*'s [10], Wu *et al.*'s [25], and the proposed strategy, respectively. Fig. 3 (c) presents the real tooth contour by manual segmentation. These results showed in Fig. 3 verified that Gao *et al.*'s strategy would propagate the boundary leakage error to the initial level set and Wu *et al.*'s strategy could eliminate the error with an inaccurate tooth shape prior, whereas the proposed strategy could obtain a more similar shape with the manual segmentation contour.

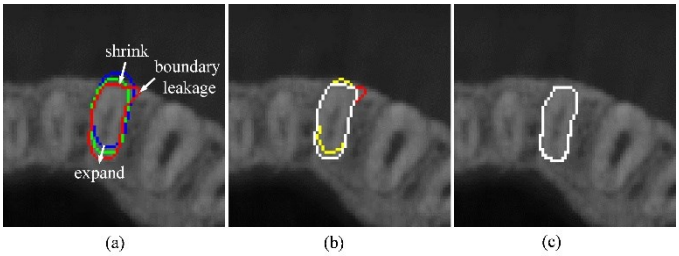

Fig. 3. Result comparison using different strategies for the tooth shape prior computation. (a) Segmented tooth contours of the previous three slices, and red, green, and blue curves denote the contours of the $(i\text{-}1)^{th}$, $(i\text{-}2)^{th}$, and $(i\text{-}3)^{th}$ slice, respectively. (b) Computed shape prior using different strategies, and red, white, and yellow curves denote results of Gao *et al.*'s [8], Wu *et al.*'s [25] and the proposed strategy, respectively. (c) The reference tooth contour of current slice by manual segmentation.

2) Neighboring Tooth Separation using the Radon Transform

Neighboring teeth may touch each other, resulting in missing of their common boundary. In order to obtain individual tooth contour, this study applied the Radon transform to extract a line to separate neighboring teeth into independent ones [26]. Then each tooth can be segmented individually from the corresponding side of the line using a single level set.

The Radon transform of a given image $I(x_1, x_2)$ $(x_1, x_2 \in \Re)$ represents a collection of one dimensional line integral (i.e. projection) of image intensity in various directions:

$$R(\theta,\rho)\left(I(x_1,x_2)\right) = \int_{-\infty}^{+\infty}\int_{-\infty}^{+\infty} I(x_1,x_2)\delta(\rho-x_1\cos\theta-x_2\sin\theta)\,dx_1dx_2 \tag{8}$$

where θ denotes the angle between the perpendicular direction of line integral and the x_1-axis, and ρ denotes the perpendicular offset of the line integral.

Assuming that neighboring teeth can be separated by a straight line, the separation line of neighboring teeth corresponds to a local minimum point $R(\theta_0, \rho_0)$ in the Radon transform as the image projection at the separation line arrives minimum. Thus the separation line extraction is equivalent to search a constraint local minimum among the Radon transform. The shape priors of the neighboring teeth were used to provide constraint for the position and direction of the separation line.

3) Local Level Set Model for Tooth Contour Segmentation

This study integrated the tooth shape prior into the geodesic active contour model [27] to construct the local level set model for tooth contour segmentation from alveolar bone, and the corresponding energy could be written as

$$E(\phi)=\int g\delta_\varepsilon(\phi)|\nabla\phi|dx+\beta\int\left(H_\varepsilon(\phi)-H_\varepsilon(\phi_0)\right)^2dx \tag{9}$$

where β is a positive weight, and ϕ_0 denotes the signed distance function of the tooth shape prior computed from previous

This article has been accepted for publication in a future issue of this journal, but has not been fully edited. Content may change prior to final publication. Citation information: DOI 10.1109/JBHI.2017.2709406, IEEE Journal of Biomedical and Health Informatics

segmented slices by (7). The first term is an edge term coming from the geodesic active contour [27]. Based on the knowledge that the image intensity of tooth is relatively higher than that of alveolar bone, this study incorporates the intensity information into the edge indictor such that the edge indicator would drive the level set curve evolve and stop at the boundary with large image gradient and high intensity to prevent the level set curve invade into alveolar bone. The second term is a tooth shape prior term and is defined as the dissimilarity of two shapes [28] represented by their embedding level set functions to prevent the level set curve evolve too far from the initial contour. One advantage of the definition is that the results mainly depend on the sign of the embedded level set function, and one does not need to constrain the level set function to the signed distance function.

The commonly used edge indicator (6) would stop the level set curve evolve at the boundary with largest image gradient. However, in dental CT images the real tooth boundary is not always located at the position with the largest image gradient. Since the tooth region has relatively higher intensity than surrounding alveolar bone, this study incorporates the intensity information into the edge indictor such that the edge indicator would stop the level set curve evolve at the boundary with large image gradient and high intensity. Additionally, as suggested in [9] [10], the gradient direction detection is helpful to guide the level set curve evolve toward the real tooth boundary. Thus, this study defines the following refined edge indicator with intensity information and gradient direction detection

$$g(x)=\begin{cases}\dfrac{0.5}{1+|\nabla G_s * I(x)|^2}+0.5\left(1-I_N(x)\right)^3, & \nabla I_G\cdot\nabla\phi\geq 0\\ 1, & \nabla I_G\cdot\nabla\phi<0\end{cases} \tag{10}$$

where I_N denotes normalized image and is defined as

$$I_N(x)=\begin{cases}\dfrac{I(x)-\min(I)}{u_0}, & I(x)<u_0+\sigma_0\\ 1, & I(x)\geq u_0+\sigma_0\end{cases} \tag{11}$$

where u_0 and σ are the mean and standard deviation of tooth intensity computed from the tooth shape prior, respectively.

The energy function (9) could be minimized by an explicit iteration scheme using the following gradient flow

$$\frac{\partial\phi}{\partial t}=\delta_\varepsilon(\phi)\,div\left(g\frac{\nabla\phi}{|\nabla\phi|}\right)-2\beta\delta_\varepsilon(\phi)\left(H_\varepsilon(\phi)-H_\varepsilon(\phi_0)\right) \tag{12}$$

In the local level set model, the weighting parameter β balances the contribution of edge term and shape prior term, and its value will affect the tooth segmentation accuracy. The model with a smaller value of β has a stronger curve evolution force to extract week tooth boundary according the image information but may suffer from boundary leakage. The model with a larger value of β has a stronger shape constraint force to prevent level set curve evolve far from the initial contour and may fail to extract real tooth boundary due to the week force of curve evolution. In the implementation, the segmentation of anterior teeth needs a relatively high value of β to prevent the level set curve invade into alveolar bone, and the segmentation of posterior teeth needs a relatively small value of β to adapt the complicated topological changes.

Conventional level set method needs a re-initialization procedure which is time consuming to prevent the level set from being too steep or flat. This study regularizes the level set after each iteration by convolving the level set function with a Gaussian filter [29]. The regularization based on Gaussian filter not only smoothed the active contour but also eliminated the need for level set re-initialization.

Compared to the previous works [10] [13], the energy function (9) does not include a region term with image intensity information as different branches of tooth split naturally in the bone tissue segmentation step, and the level set curve only needs to evolve within a relatively small region of the initial contour to extract tooth boundary. Another difference is that in this study the image intensity information is incorporated into the edge indictor to prevent the level set curve invade into alveolar bone.

4) Tooth Segmentation of the Starting Slice

For the starting slice, the tooth contour propagation strategy is infeasible as there is no tooth shape prior. Since this slice is selected from crown part where no alveolar bone connects with tooth, tooth contours can be directly extracted from the results of the first step segmentation. In the results of the first step segmentation, the regions which intersect with manually drawn seed points are regarded as valid tooth regions. A line is computed to separate each pair of possible touching neighboring teeth based on the Radon transform. In the computation of the separation line, the seed points were used to provide constraint for the position and direction.

III. Experiments

A. Dataset and Evaluation Method

CBCT images were acquired from sixteen subjects and used to test the performance of the proposed method. These images were scanned by a CT scanner (NewTom VG, Italy) with a voxel size of 0.25 mm. The scanning parameters of tested images were 120 kV, 5 mA, and with 6 s as time of exposure. All the images were scanned when the subjects' teeth were in an open bite position to make sure that lower and upper teeth do not overlap in any slice. There are no metal artifacts in these images. Before being segmented, the volumetric images have been reoriented manually such that most slices in the transverse plane contain all tooth contours. For all the tested images, the parameter λ in (5) was set to be 10.0, and parameters Δt and β in (12) were set to be 5.0 and 0.1, respectively. This study was reviewed and approved by Institutional Review Board of Shenzhen Institutes of Advanced Technology, Chinese Academy of Sciences. Written informed consents of the subjects were obtained.

Manual segmentation results by experienced clinicians were used as the gold standard to be compared to the algorithm results. Three performance metrics were used to estimate the

This article has been accepted for publication in a future issue of this journal, but has not been fully edited. Content may change prior to final publication. Citation information: DOI 10.1109/JBHI.2017.2709406, IEEE Journal of Biomedical and Health Informatics

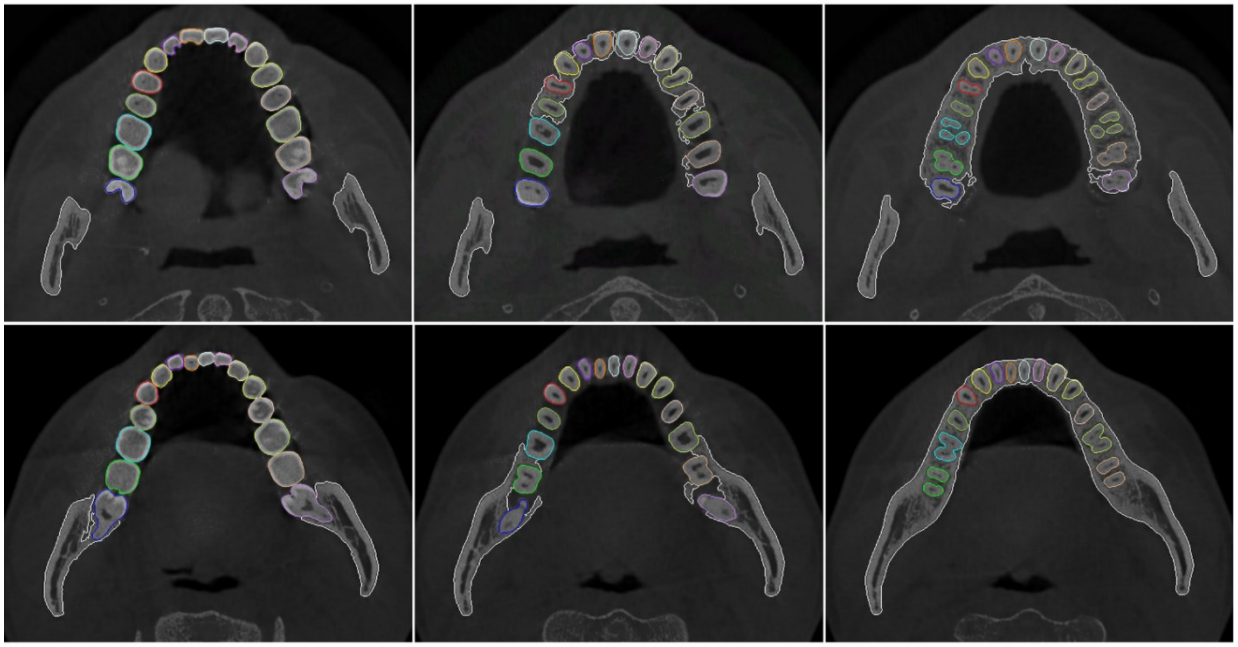

Fig. 4. Results of tooth and alveolar bone segmentation. Upper: maxillary slices, lower: mandible slices. The color curves denote individual tooth contours, and the white curves denote outer contours of alveolar bone.

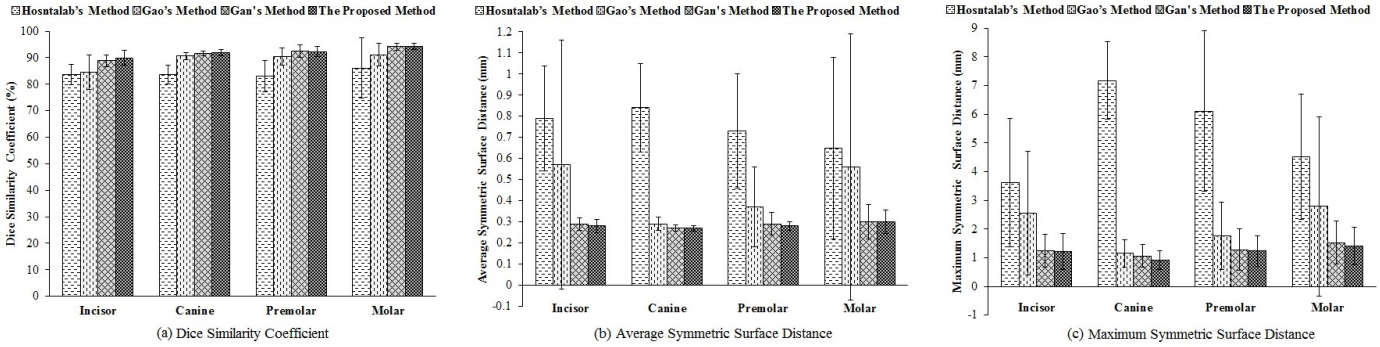

Fig. 5. Comparison of tooth segmentation accuracy using different methods.

segmentation accuracy. They included one volume overlap metrics, Dice similarity coefficient (DSC, %), and two surface distance metrics, average symmetric surface distance (ASSD, mm), and maximum symmetric surface distance (MSSD, mm). The three performance metrics were defined as:

$$DSC = \frac{2V_R \cap V_A}{V_R + V_A} \tag{13}$$

$$ASSD(S_R, S_A) = mean\left\{mean\left\{dist\left(a, S_R\right), a \in S_A\right\}, mean\left\{dist\left(r, S_A\right), r \in S_R\right\}\right\} \tag{14}$$

$$MSSD(S_R, S_A) = max\left\{max\left\{dist\left(a, S_R\right), a \in S_A\right\}, max\left\{dist\left(r, S_A\right), r \in S_R\right\}\right\} \tag{15}$$

where V_R and V_A are the volumes of objects of gold standard and algorithm segmentation, respectively, S_R and S_A are the surfaces of objects of gold standard and algorithm segmentation, respectively, $dist(a, S_R)$ is the nearest Euclidean distance from a surface point a to the surface S_R, $mean\{\bullet\}$ and $max\{\bullet\}$ are the arithmetical average and maximum operator, respectively.

The presented method was implemented using MATLAB code and ran on a DELL graphic workstation (Win 7, Intel E5-2643 3.3 GHz CPU, 16 GB RAM). The processing time for segmenting the tested images was recorded to assess the efficiency of the proposed method.

B. Qualitative Results

Fig. 4 shows tooth and alveolar bone segmentation results using the proposed method for sample slices of crown, tooth neck, and root parts. It can be observed that the proposed method could segment both individual tooth and alveolar bone successfully and the visual segmentation accuracy was satisfying.

C. Quantitative Results and Comparison

The quantitative tooth and alveolar bone segmentation accuracy of the proposed method on the tested images is listed in Table 1. The average symmetric surface distance error is approximated to one voxel size which means that the proposed method archives segmentation accuracy of pixel level.

This article has been accepted for publication in a future issue of this journal, but has not been fully edited. Content may change prior to final publication. Citation information: DOI 10.1109/JBHI.2017.2709406, IEEE Journal of Biomedical and Health Informatics

TABLE I
TOOTH AND ALVEOLAR BONE SEGMENTATION ACCURACY OF THE PROPOSED METHOD.

Tissue	Metrics		
	DSC (%)	ASSD (mm)	MSSD (mm)
Incisor	89.98 ± 2.80	0.28 ± 0.03	1.21 ± 0.63
Canine	91.86 ± 1.22	0.27 ± 0.01	0.92 ± 0.32
Premolar	92.34 ± 1.95	0.28 ± 0.02	1.23 ± 0.54
Molar	94.26 ± 1.10	0.30 ± 0.06	1.41 ± 0.66
Alveolar Bone	95.64 ± 2.12	0.25 ± 0.02	1.07 ± 0.36

In addition, the performance of the proposed method was compared to three other methods: Honstalab *et al.*'s method [3], Gao *et al.*'s method [10], and Gan *et al.*'s method [13]. Since the previous three methods only implemented tooth segmenation, only the tooth segmentation results using different methods were compared. Fig. 5 shows the quantitative comparision of tooth segmentation accuracy using different methods. We can see that the segmentation accuracy of the proposed method outperforms the previous methods. Compared to Honstalab *et al.*'s and Gao *et al.*'s methods, the accuracy improvement of the proposed method is significant (p<0.05, t-test).

The computation time of the proposed method for segmenting one set of volumetric images was 4.23±0.67 min. The comparison of computation time when using different methods is shown in Fig. 6. It can be seen that although the proposed method needs two steps to complete the segmentation, it is more efficient than Gao *et al.*'s and Gan *et al.*'s methods. The reason is that, in the proposed method the Split Bregman method makes the minimization of the global convex level set model in the first step much faster than (more than 10 times) the gradient decent iteration in (2), and the local level set in the second step is much less complicated than models used in Gao *et al.*'s method and Gan *et al.*'s method. As a result, the proposed method is more efficient than Gao *et al.*'s and Gan *et al.*'s method.

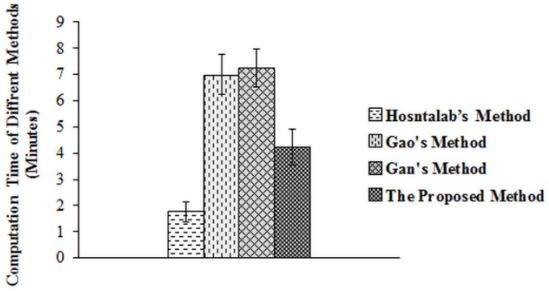

Fig. 6. Computation time comparison of different methods for segmenting one set of images.

D. Visualization

Individual 3D models of tooth and alveolar bone of one subject reconstructed from results segmented using the proposed method is presented in Fig. 7. These models provide subject's complete information of both tooth and alveolar bone, and can be used for orthodontic treatment planning and biomechanics simulation.

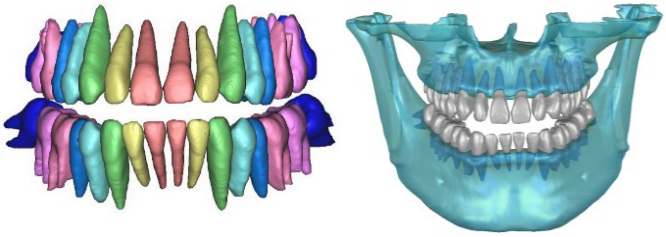

Fig. 7. 3D models of individual teeth and alveolar bones of one subject reconstructed from results segmented using the proposed method.

IV. DISCUSSION

A. Effect of the First Step Segmentation

In the proposed method, the first step would be important in implementing the segmentation of both tooth and alveolar bone from dental CT images. After the tooth is segmented in the second step, both individual tooth and alveolar bone are obtained and the complete 3D models of tooth-alveolar bone complex can be reconstructed and applied to orthodontic treatment planning and biomechanical simulation.

In addition, the first step segmentation also facilitates the individual tooth segmentation from alveolar bone. In the slices where a tooth splits into different branches, the region between different branches is composed of non-bony tissue (soft tissue in root and air in crown). After the first step segmentation, these region are segmented as background, and different branches split naturally. Thus, methods or models which cannot deal with topological changes are feasible to segment tooth from connected region of tooth and alveolar bone.

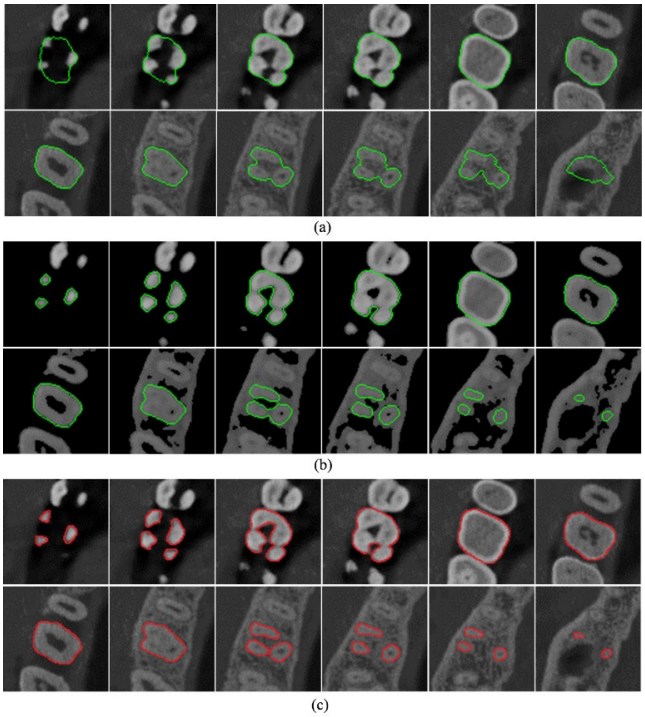

Fig. 8. Comparison of segmentation results using the second step segmentation directly and the two-step segmentation. (a) Results by using the second step segmentation directly. (b) Results by using the two-step segmentation. (c) Real tooth contours by manual segmentation.

This article has been accepted for publication in a future issue of this journal, but has not been fully edited. Content may change prior to final publication. Citation information: DOI 10.1109/JBHI.2017.2709406, IEEE Journal of Biomedical and Health Informatics

Fig. 8 shows comparison of segmentation results using the second step segmentation directly and the proposed two-step segmentation for a maxillary first left molar. The local level set model in the second step is an edged-based model. Its level set curve is hard to evolve into the region with deep concave structure, thus cannot deal with the topological change of tooth. The results shown in Fig. 8 (a) indicate that only using the second step segmentation failed to segment the tooth contours from these slices with different branches. With the proposed two-step segmentation method, the different branches of the teeth were successfully extracted from the CT images, as shown in Fig. 8 (b).

B. Necessity of the Integrated Intensity Information in the Edge Detector

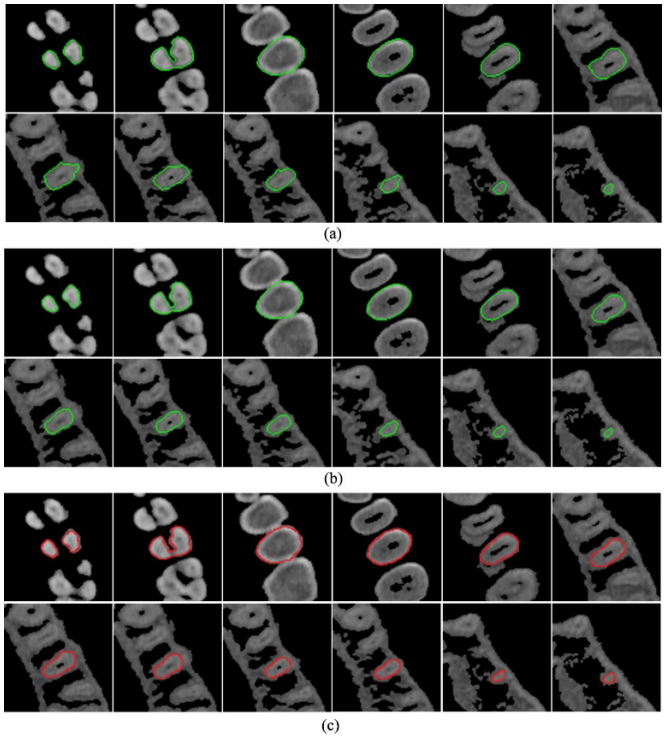

Fig. 9. Comparison of segmentation results with and without image intensity in the edge indicator. (a) Results without image intensity in the edge indicator. (b) Results with image intensity in the edge indicator. (c) Real tooth contours by manual segmentation.

The conventional edge indicator completely depends on the image gradient to drive the level set curve evolve and stop at the boundary with the largest image gradient. However, in dental CT images, the real tooth boundary is not always located at the position with the largest image gradient. As tooth region has relatively higher intensity than surrounding alveolar bone, this study incorporates the intensity information into the edge indicator such that the refined edge indicator drives the level set curve evolve and stops at the boundary with large gradient and high intensity. Fig. 9 (a) shows the segmentation results of a maxillary right premolar using the proposed method but no intensity information is incorporated into the edge indicator. The results show that without the image intensity information, the edge indicator failed to extract the tooth contours of some slices accurately. With the image intensity, the edge indicator could obtain more accurate tooth contours, as shown in Fig. 9 (b).

C. Contribution and Limitation

3D models of tooth-alveolar bone complex are needed in treatment planning and simulation for computer-aided orthodontics. However, conventional orthodontic treatment mainly uses tooth model to perform diagnosis and treatment planning and alveolar bone is less used which may cause undesired side effects. In the treatment planning, the alveolar bone is necessary to align tooth roots well since it provides reference for the potential position and direction of root. If only using tooth models to perform a treatment planning, there is a risk that the planned tooth roots may be not surrounded by the alveolar bone and tooth loss will occur after the orthodontic treatment. In addition, the dental biomechanics involves tooth, periodontal ligament, and alveolar bone. Anatomically accurate models of both bone and alveolar bone are needed for accurate simulation [30]. Due to less application of alveolar bone, previous dental CT image processing method focused on tooth, and alveolar bone was not considered. This study developed a method to segment both tooth and alveolar bone from CT images for their model reconstruction, and will benefit the computer-aided orthodontic treatment.

In this study, we only considered the segmentation of dental CT images scanned when the subjects' teeth were in an open bite position and there are no metal artifacts in these images. The crown segmentation from these images scanned in a close bite position and/or with metal artifacts is especially difficult, and has been addressed in our previous works [26] [31].

The proposed method segmented tooth contours from volumetric CT images using a slice-by-slice way. This kind of methods may fail to segment the angled teeth due to the low coherence between contours of adjacent slices. To segment the dental CT images with angled teeth, one possible method is to manually re-orientate the volumetric images for different teeth. In the future work we will focus on the extension of the proposed method for the robustness segmentation of angled tooth.

V. Conclusion

Computer-aided orthodontic treatment needs complete 3D models of tooth-alveolar bone complex, which requires the segmentation of tooth and alveolar bone from the dental CT images for model reconstruction. However, existing methods only studied the segmentation of teeth. This study presented a level set based method to segment both tooth and alveolar bone. The proposed method performed the segmentation through two steps, in which a global convex level set model was first used to segment the connected region of tooth and alveolar bone, and then the individual tooth and alveolar bone were separated from the connected region based on the Radon transform and a local level set model. Experimental results showed that the presented method could successfully extract the teeth and alveolar bones from the CT images. In addition, the performance of the proposed method in segmenting tooth outperformed state of the art tooth segmentation methods in terms of segmentation

accuracy. These results suggest that the newly proposed method would be used to reconstruct the 3D models of tooth-alveolar complex, which will benefit the computer-aided orthodontic treatment.

REFERENCES

[1] H. Akhoondali, R. A. Zoroofi, and G. Shirani, "Rapid automatic segmentation and visualization of teeth in CT-scan data," *J. Appl. Sci.*, vol. 9, no. 11, pp. 2031-2044, Nov. 2009.

[2] S. Keyhaninejad, R. A. Zoroofi, S. K. Setarehdan, and G. Shirani, "Automated segmentation of teeth in multi-slice CT images," in *Proc. IET Int. Conf. Vis. Inf. Eng.*, Bangalore, India, 2006, pp. 339–344.

[3] M. Hosntalab, R. A. Zoroofi, A. A. Tehrani-Fard, and G. Shirani, "Segmentation of teeth in CT volumetric dataset by panoramic projection and variational level set," *Int. J. Comput. Ass. Rad.*, vol. 3, no. 3-4, pp. 257–265, Sep. 2008.

[4] J. Keustermans, D. Vandermeulen, and P. Suetens, "Integrating statistical shape models into a graph cut framework for tooth segmentation," In *Machine Learning in Medical Imaging (LNCS 7588)*, Berlin, Germany: Springer, 2012, pp. 240-247.

[5] L. T. Hiew, S. H. Ong, and K. W. C. Foong, "Tooth segmentation from cone-beam CT using graph cut," in *Proc. Sec. APSIPA Ann. Summit and Conf.*, Biopolis, Singapore, 2010, pp. 272-275.

[6] S. Barone, A. Paoli, and A. V. Razionale, "CT segmentation of dental shapes by anatomy-driven reformation imaging and B-spline modelling," *Int. J. Numer. Method Biomed. Eng.*, vol 32, no. 6, pp. e02747, Jun. 2016.

[7] Y. Pei, X. Ai, H. Zha, T. Xu, and G. Ma, "3D exemplar-based random walks for tooth segmentation from cone-beam computed tomography images," *Med. Phys.*, vol. 43, no. 9, pp. 5040-5050, Sep. 2016.

[8] H. Heo and O. Chae, "Segmentation of tooth in CT images for the 3D reconstruction of teeth," in *Proc. SPIE-IS&T Elec. Imaging*, 2004, pp. 455-466.

[9] X. Wu, H. Gao, H. Heo, O. Chae, J. Cho, S. Lee, and Y. Lee, " Improved B-spline contour fitting using genetic algorithm for the segmentation of dental computerized tomography image sequences," *J. Imaging Sci Techn.*, vol. 51, no. 4, pp. 328-336, Jul. 2007.

[10] H. Gao and O. Chae, "Individual tooth segmentation from CT images using level set method with shape and intensity prior," *Pattern Recogn.*, vol. 43, no. 7, pp. 2406-2417, Jul. 2010.

[11] H. Yau, T. Yang, and Y. Chen, "Tooth model reconstruction based upon data fusion for orthodontic treatment simulation," *Comput. Biol. Med.*, vol. 48, pp. 8-16, May 2014.

[12] D. X. Ji, S. H. Ong, and K. W. C. Foong, "A level-set based approach for anterior teeth segmentation in cone beam computed tomography images," *Comput. Biol. Med.*, vol. 50, pp. 116-128, Jul. 2014.

[13] Y. Gan, Z. Xia, J. Xiong, Q. Zhao, Y. Hu, and J. Zhang, "Towards accurate tooth segmentation from computed tomography images using a hybrid level set model," *Med. Phys.*, vol. 42, no. 1, pp. 14-27, Jan. 2015.

[14] L. Wang, K. C. Chen, Y. Gao, F. Shi, S. Liao, G. Li, S. G. F. Shen, J. Yan, P. K. M. Lee, B. Chow, N. X. Liu, J. J. Xia, and D. Shen, "Automated bone segmentation from dental CBCT images using patch-based sparse representation and convex optimization," *Med. Phys.*, vol. 41, no. 4, pp. 043503, Apr. 2014.

[15] L. Wang, Y. Gao, F. Shi, G. Li, K. Chen, Z. Tang, J. J. Xia, and D. Shen, "Automated segmentation of dental CBCT image with prior-guided sequential random forests," *Med. Phys.*, vol. 43, no. 1, pp. 336-346, Jan. 2016.

[16] Z. Xia and J. Chen, "Biomechanical validation of an artificial Tooth-PDL-Bone Complex for in-vitro orthodontic load measurement," *Angle Orthod.*, vol. 83, no. 3, pp. 410-417, Sep. 2013.

[17] S. Tang, Y. Guo, Y. Wang, W. Cao, and F. Sun, "Adaptive cosegmentation of pheochromocytomas in CECT images using localized level set models," *IEEE J. Biomed. Health Inform.*, vol. 20, no. 2, pp. 549-562, Mar. 2016.

[18] J. Pang J, J. B. Driban, T. E. McAlindon, J. G. Tamez-Pe˜na, J. Fripp, and E. L. Miller, "On the use of coupled shape priors for segmentation of magnetic resonance images of the knee," *IEEE J. Biomed. Health Inform.*, vol., no. 3, 19 (3), pp. 1153-1167, May 2015.

[19] X. Qin, X. Li, Y. Liu, H. Lu, and P. Yan, "Adaptive shape prior constrained level sets for bladder MR image segmentation," *IEEE J. Biomed. Health Inform.*, vol. 18, no. 5, pp. 1707-1716, Sep. 2014.

[20] L. A. Vese and T. F. Chan, "A multiphase level set framework for image segmentation using the Mumford and Shah model," *Int. J. Comput. Vis.*, vol. 50, no. 3, pp. 271-293, Dec. 2002.

[21] C. Li, C. Kao, J. C. Gore, and Z. Ding, "Minimization of region-scalable fitting energy for image segmentation," *IEEE Trans. Image Process.*, vol. 17, no. 10, pp. 1940-1949, Oc. 2008.

[22] T. F. Chan TF and L. A. Vese, "Active contours without edges," *IEEE Trans. Image Process.*, vol. 10, no. 2, pp. 266-277, Feb. 2001.

[23] T. F. Chan, S. Esedoglu, and M. Nikolova, "Algorithms for finding global minimizers of image segmentation and denoising models," *SIAM J. Appl. Math.*, vol. 66, no. 5, pp. 1632-1648, Sep. 2006.

[24] T. Goldstein, X. Bresson, and S. Osher, "Geometric applications of the Split Bregman method: segmentation and surface reconstruction," *J. Sci. Comput.*, vol. 45, no. 1, pp. 272-293, Oct. 2010.

[25] W. Qiu, J. Yuan, E. Ukwatta, D. Tessier, and A. Fenster, "Three-dimensional prostate segmentation using level set with shape constraint based on rotational slices for 3D end-firing TRUS guided biopsy," *Med. Phys.*, vol. 40, no. 7, pp. 072903, Jul. 2013.

[26] Z. Xia, Y. Gan, J. Xiong, Q. Zhao, and J. Chen, "Crown segmentation from computed tomography images with metal artifacts," *IEEE Signal Process. Lett.*, vol. 23, no. 5, pp. 678-682, May. 2016.

[27] V. Caselles, R. Kimmel R, and G. Sapiro, "Geodesic active contours," *Int. J. Comput. Vis.*, vol. 22, no. 1, pp.61-79, Feb. 1997.

[28] T. Chan and W. Zhu, "Level set based shape prior segmentation," *in Proc. IEEE Conf. Computer Vision and Pattern Recognition,* San Diego, CA, 2005, pp. 1164-1170.

[29] K. Zhang, H. Song, and L. Zhang, "Active contours driven by local image fitting energy," *Pattern Recogn.*, vol. 43, no. 4, pp. 1199-1206, Apr. 2010.

[30] Z. Liao, J. Chen, Z. Zhang, W. Li, M. Swain, and Q. Li, "Computational modeling of dynamic behaviors of human teeth," *J. Biomech.*, vol. 48, no. 16, pp. 4214-4220, Dec. 2015.

[31] Z. Xia, Y. Gan, L. Chang, J. Xiong, and Q. Zhao, "Individual tooth segmentation from CT images scanned with contacts of maxillary and mandible teeth," *Comput. Meth. Programs Biomed.*, vol. 138, pp. 1-12, Jan. 2017.